

c.1

**ARCHIVE COPY
DO NOT LOAN**

Experimental Studies
of Multiple-Scattered Light
from Latex Spheres

D. P. Weaver, B. P. Curry, and J. W. L. Lewis
ARO, Inc.

October 1979

Final Report for Period October 1976 — November 1978

Approved for public release; distribution unlimited.

Property of U. S. Air Force
AEDC LIBRARY
F40600-77-C-0003

**ARNOLD ENGINEERING DEVELOPMENT CENTER
ARNOLD AIR FORCE STATION, TENNESSEE
AIR FORCE SYSTEMS COMMAND
UNITED STATES AIR FORCE**

AEDC TECHNICAL LIBRARY



5 0720 00034 4067

NOTICES

When U. S. Government drawings, specifications, or other data are used for any purpose other than a definitely related Government procurement operation, the Government thereby incurs no responsibility nor any obligation whatsoever, and the fact that the Government may have formulated, furnished, or in any way supplied the said drawings, specifications, or other data, is not to be regarded by implication or otherwise, or in any manner licensing the holder or any other person or corporation, or conveying any rights or permission to manufacture, use, or sell any patented invention that may in any way be related thereto.

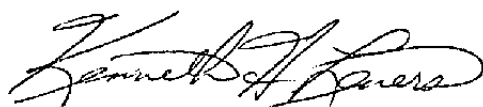
Qualified users may obtain copies of this report from the Defense Documentation Center.

References to named commercial products in this report are not to be considered in any sense as an indorsement of the product by the United States Air Force or the Government.

This report has been reviewed by the Information Office (OI) and is releasable to the National Technical Information Service (NTIS). At NTIS, it will be available to the general public, including foreign nations.

APPROVAL STATEMENT

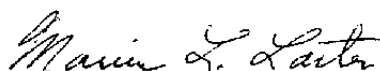
This report has been reviewed and approved.



KENNETH H. LENERS, Captain, USAF
Project Manager
Directorate of Technology

Approved for publication:

FOR THE COMMANDER



MARION L. LASTER
Director of Technology
Deputy for Operations

UNCLASSIFIED

REPORT DOCUMENTATION PAGE		READ INSTRUCTIONS BEFORE COMPLETING FORM
1. REPORT NUMBER AEDC-TR-79-60	2. GOVT ACCESSION NO.	3. RECIPIENT'S CATALOG NUMBER
4. TITLE (and Subtitle) EXPERIMENTAL STUDIES OF MULTIPLE-SCATTERED LIGHT FROM LATEX SPHERES	5. TYPE OF REPORT & PERIOD COVERED Final Report - October 1976 - November 1978	
	6. PERFORMING ORG. REPORT NUMBER	
7. AUTHOR(s) D. P. Weaver, B. P. Curry, and J. W. L. Lewis, ARO, Inc., a Sverdrup Corporation Company		8. CONTRACT OR GRANT NUMBER(s)
9. PERFORMING ORGANIZATION NAME AND ADDRESS Arnold Engineering Development Center/DOT Air Force Systems Command Arnold Air Force Station, Tennessee 37389		10. PROGRAM ELEMENT, PROJECT, TASK AREA & WORK UNIT NUMBERS Program Element 62302F
11. CONTROLLING OFFICE NAME AND ADDRESS Air Force Rocket Propulsion Laboratory/PACP Edwards Air Force Base, California 93523		12. REPORT DATE October 1979
14. MONITORING AGENCY NAME & ADDRESS (if different from Controlling Office)		13. NUMBER OF PAGES 28
		15. SECURITY CLASS. (of this report) UNCLASSIFIED
15a. DECLASSIFICATION/DOWNGRADING SCHEDULE N/A		15. SECURITY CLASS. (of this report)
		15a. DECLASSIFICATION/DOWNGRADING SCHEDULE N/A
15. DISTRIBUTION STATEMENT (of this Report) Approved for public release; distribution unlimited.		
17. DISTRIBUTION STATEMENT (of the abstract entered in Block 20, if different from Report)		
18. SUPPLEMENTARY NOTES Available in DDC		
19. KEY WORDS (Continue on reverse side if necessary and identify by block number) light scattering refractive index optics measurements models spheres exhaust plumes latex visibility particle size lasers		
20. ABSTRACT (Continue on reverse side if necessary and identify by block number) This report presents the results of a series of light- scattering measurements on small, spherical particles of a known size distribution and index of refraction. The purpose of the study is to provide additional data for the evaluation of the multiple-scattering model used in a plume visibility code currently being developed for the Air Force. Measurements of both singly and multiply scattered laser radiation from aqueous		

UNCLASSIFIED

UNCLASSIFIED

20. ABSTRACT (Continued)

suspensions of spherical latex particles were performed at several optical depths. Included are descriptions of the light-scattering apparatus and sample preparation techniques used in the study. Also, sample results of the experiments are presented in graphical form with normalized scattering intensity as a function of scattering angle.

PREFACE

The work reported herein was conducted by the Arnold Engineering Development Center (AEDC), Air Force Systems Command (AFSC), under the sponsorship of the Air Force Rocket Propulsion Laboratory (AFRPL)/(PACP). The results of the research were obtained by ARO, Inc., AEDC Division (a Sverdrup Corporation Company), operating contractor for the AEDC, AFSC, Arnold Air Force Station, Tennessee, under ARO Project No. V34S-R9A. Captain Stanislaus L. Ludwig (CF) was the Air Force project manager, and Lt. Eric Lund was the AFRPL project manager. The data analysis was completed on November 27, 1978, and the manuscript was submitted for publication on July 7, 1979.

CONTENTS

	<u>Page</u>
1.0 INTRODUCTION	5
2.0 EXPERIMENTAL APPARATUS AND PROCEDURES	
2.1 Source Radiation	6
2.2 Light-Scattering Apparatus	8
2.3 Scattering Detector System	13
2.4 Sample Preparation	15
2.5 Transmission Measurements	17
2.6 Data Acquisition Procedure	17
3.0 RESULTS AND DISCUSSION	
3.1 Correction Terms	19
3.2 Sample Data	21
4.0 CONCLUSIONS	21
REFERENCES	26

ILLUSTRATIONS

Figure

1. Source Optical System	7
2. Source Beam Profile	8
3. Light-Scattering Apparatus-General View	9
4. Light-Scattering Apparatus-Planar Geometry	10
5. Light-Scattering Apparatus-Cylindrical Geometry	11
6. Transmission Results for 0.220- μ m-diam Particles	13
7. Receiver Optical System	14
8. Transmission Results for 0.220- μ m-Diam Particles	18
9. Single-Scattering Data Comparison with Stray Light Background	20
10. Single-Scattering Alignment Comparison	22
11. Experimental Data, Planar Geometry, $\tau = 0.073$	23
12. Experimental Data, Planar Geometry, $\tau = 0.50$	23
13. Experimental Data, Planar Geometry, $\tau = 1.00$	24
14. Experimental Data, Cylindrical Geometry, $\tau = 0.073$	24
15. Experimental Data, Cylindrical Geometry, $\tau = 0.50$	25
16. Experimental Data, Cylindrical Geometry, $\tau = 1.00$	25
NOMENCLATURE	27

1.0 INTRODUCTION

A rocket exhaust plume may be observed visually because of the interaction of the plume exhaust species with incident or impinging visible radiation. Observation of the primary smoke region of the exhaust plume is made possible not only by spontaneous emission of the exhaust species but also by the scattering of the incident visible radiation by the comparatively large particulate matter entrained within the plume. In contrast, the time-delayed formation of the contrail-like, secondary smoke of the exhaust can be detected visually because of the scattering of incident visible radiation by small, supramolecular species that result from the interaction of the exhaust plume species with the ambient atmosphere. Further, the concentration of these supramolecular scatterers, in conjunction with the spatial size of the secondary smoke region, becomes sufficiently great that a photon scattered from the incident radiation has a strong chance of being scattered one or more additional times before it emerges from the secondary smoke region. The difficulty of providing accurate predictions of such multiple-scattering processes is well known; for the prediction of detectability of secondary smoke formation, this difficulty is increased by the complications of gas-dynamic mixing and chemical kinetics of the plume-atmosphere mixture and also by the need to describe the interaction of the plume scatterers with the spectrally broad-band solar source for a wide range of incidence and viewing angles.

As part of an Air Force Rocket Propulsion Laboratory (AFRPL) program to develop and verify computer-based models predicting plume visibility, experimental results were obtained of the angular dependence of the intensity of radiation following a multiple-scattering process for which the particle index of refraction and size distribution function were known to be accurate and for which the complications of turbulent gas mixing and chemical kinetics processes did not exist. Further, it was desired that the incident radiation be monochromatic but variable in wavelength and that it possess geometrical characteristics that would make possible a verification of portions of the calculated predictions of plume visibility. This report describes the experimental methodology used for this study and presents sample data results.

2.0 EXPERIMENTAL APPARATUS AND TECHNIQUES

For the evaluation, the multiple-scattering model data were obtained in a series of light-scattering measurements of monodisperse and polydisperse, aqueous suspensions of polystyrene latex spheres supplied by Dow Chemical Company. These suspensions were composed of particles of known optical properties and known size distributions; the particle diameters ranged from 0.1 to 1.0 micron (μm). The measurements were made using a light-scattering instrument developed at AEDC. A light-scattering cell was especially constructed to provide for aqueous suspension of the sample in the variety of

geometrical configurations required for model evaluation. The particle concentration of the samples was such that it produced multiple-radiative-scattering effects of the magnitude anticipated for application of the plume visibility model. The laser source radiation was modified to provide the wide, monochromatic, uniform and parallel beam of specific injection angle necessary for model comparison. Incident wavelengths were confined to the visible region. In the following sections detailed descriptions of the light-scattering apparatus, the sample preparation techniques, and the data reduction procedure are presented.

2.1 SOURCE RADIATION

Comparison of the predictions of the plume visibility model with the multiple-scattering measurements required the construction of an experimental system meeting the requirements of an incident plane radiation wave much wider than the appropriate characteristic distance of the scattering medium. The system used to produce this source beam is shown schematically in Fig. 1. The 2.0-mm-diam beam of 514.5-nm wavelength shown emerging from a Coherent Radiation Model CR-3 argon-ion (Ar^+) laser was directed into a series of lenses that served both to expand and then to collimate the resulting beam. Apertures in the lens system served as a spatial filter and limited the exit diameter of the beam to 25.4 mm. The resulting beam was uniform in intensity across its spatial extent to within 10 percent of its average intensity. This was verified by using a Coherent Radiation Model C212 power meter for a series of measurements of beam intensity as a function of spatial position within the beam. For these measurements the aperture of the detector's active surface area was 0.011 cm^2 , and the power was recorded as a function of the detector's position within the source beam. A sample measurement of intensity as a function of spatial location for a scan across the beam's diameter is graphed in Fig. 2.

Since the beam emerging from the laser source is polarized, measurements of scattering as a function of incident polarization were made using a half-wave polarizing plate. When measurements for a depolarized incident beam were required, a Lyot depolarizer (scrambler) was inserted into the incident laser beam path, as shown in Fig. 1. Since the polarization efficiencies of both the half-wave plate and of the scrambler are functions of wavelength, these efficiencies were measured for the wavelengths utilized in this study and were included in the final data analysis.

Further, to investigate the effect of variation of incident laser wavelength on the scattering process, a combination laser source consisting of a Coherent Radiation Model 590 dye laser pumped by the Coherent Radiation Model CR-3 argon laser was substituted for the simple CR-3 source mentioned above. For this case, Rhodamine 6G laser dye was selected; it yields dye laser output wavelengths (measured in air) in the 591.0- to

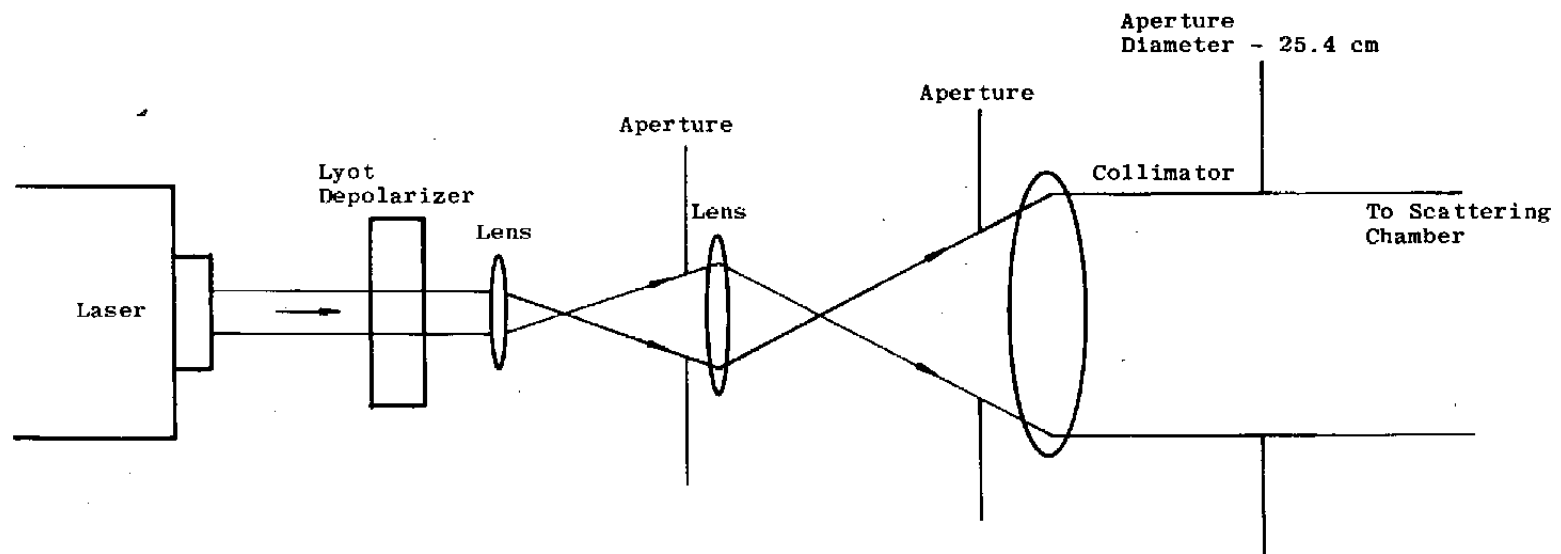


Figure 1. Source optical system.

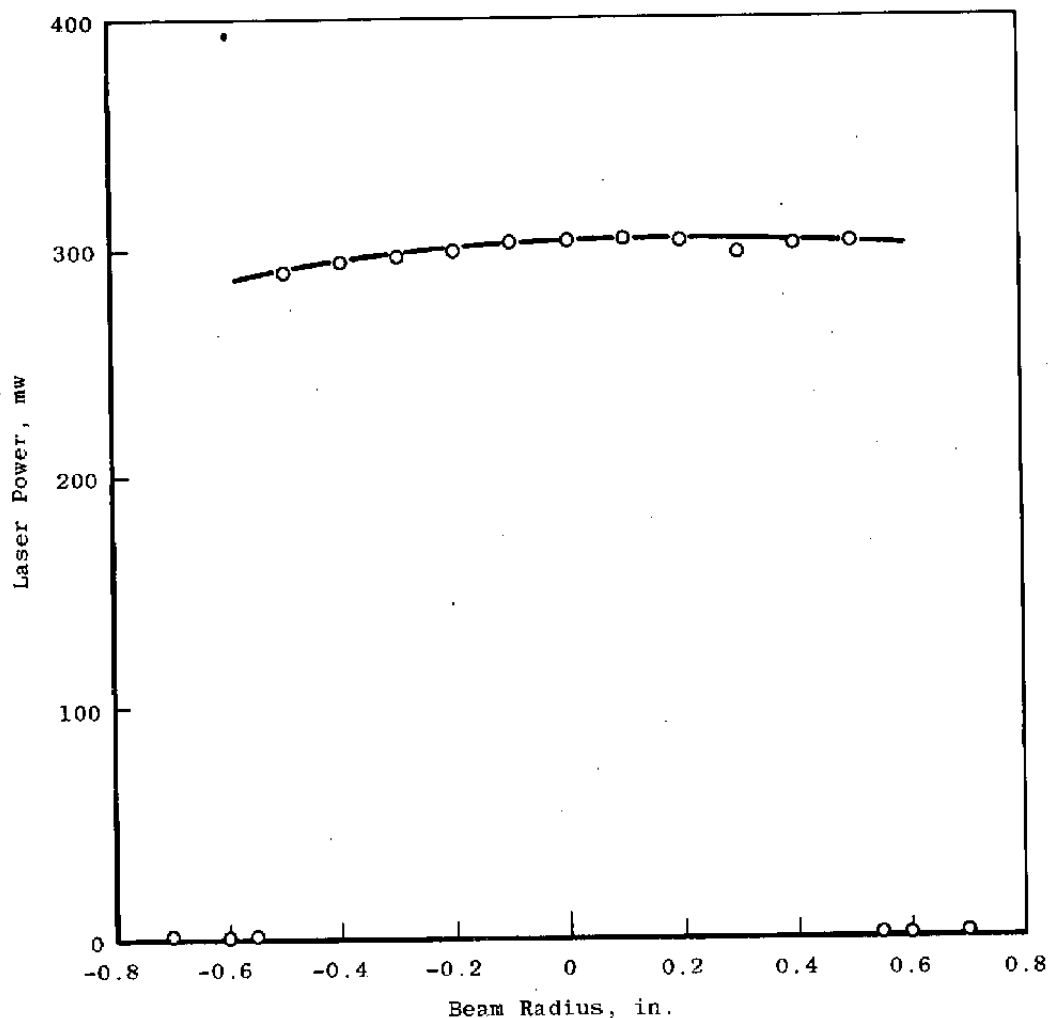


Figure 2. Source beam profile.

610.3-nm range. This combination source was placed in the same position as the Ar^+ laser shown in Fig. 1. The spatial uniformity of the dye laser beam's power density was similar to that shown for the Ar^+ laser in Fig. 2.

2.2 LIGHT-SCATTERING APPARATUS

The light-scattering apparatus used in this study is shown in Figs. 3, 4, and 5. The system was comprised of a radiation source (provided by the laser/lens system described in the section above), a special chamber containing the scatterers, and a receiver system for collecting and recording the intensity of the scattered radiation.

The scatterers, consisting of monodisperse or polydisperse latex spheres in aqueous suspension, were configured in two geometries (planar and cylindrical) representative of

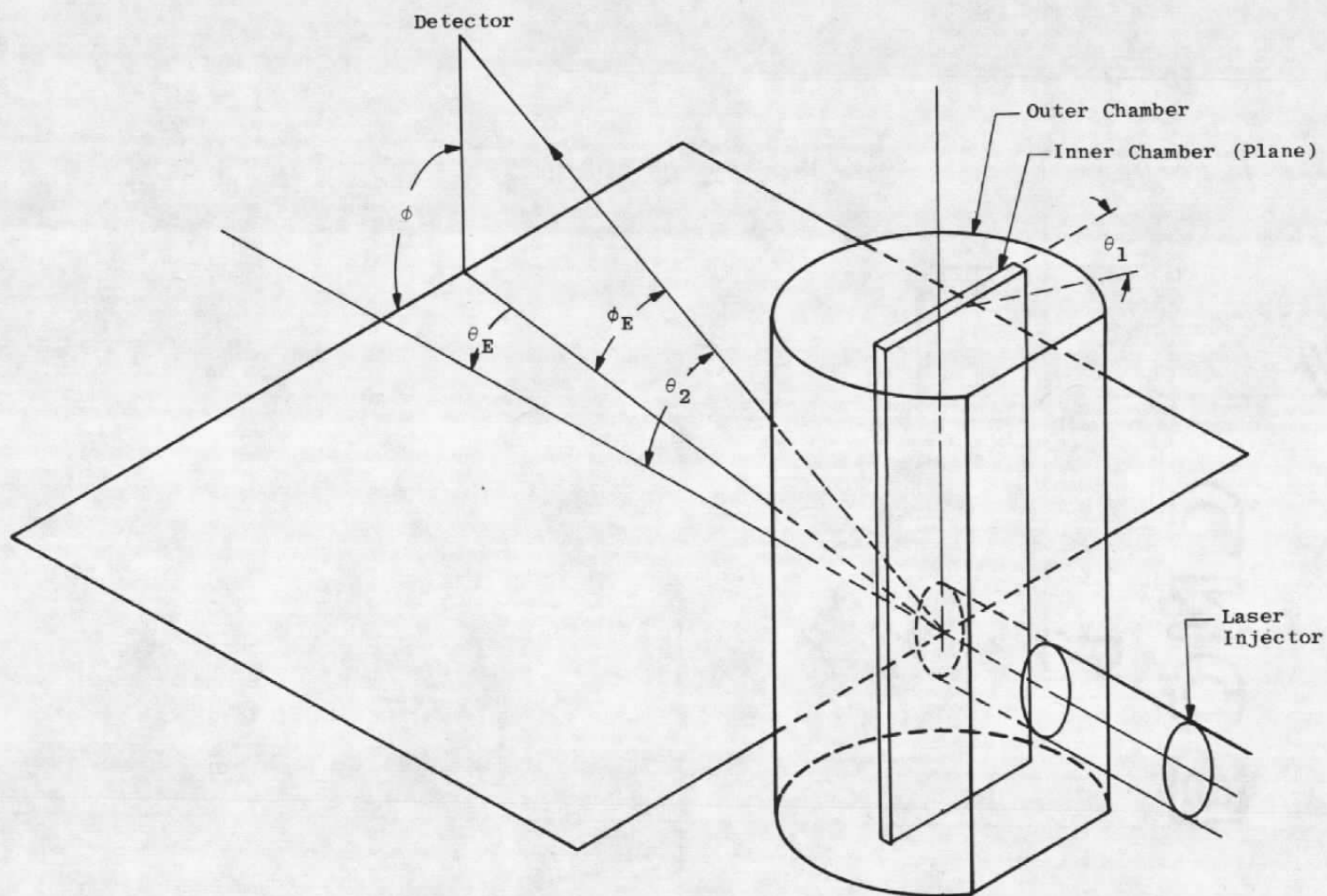


Figure 3. Light-scattering apparatus—general view.

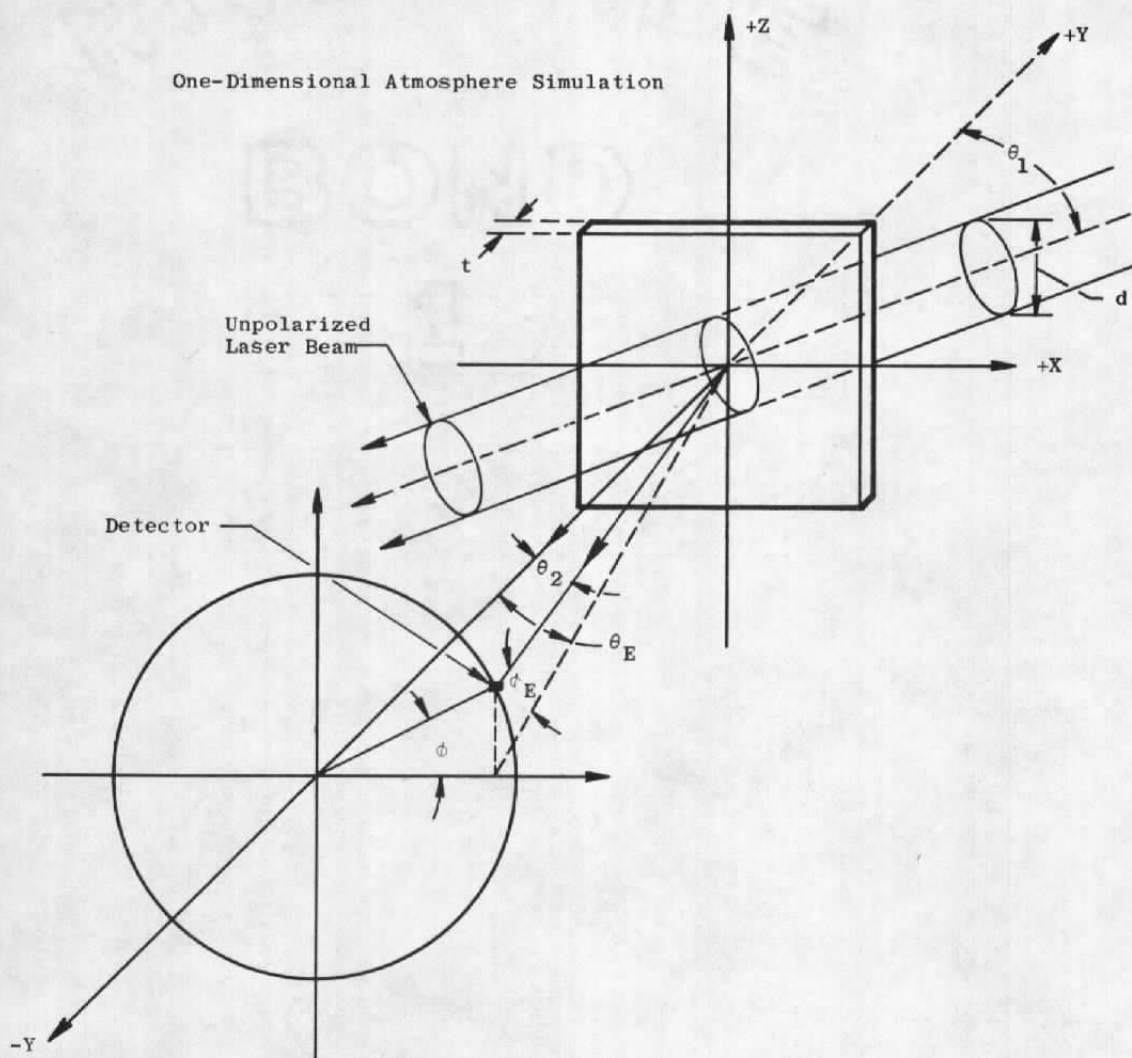


Figure 4. Light-scattering apparatus—planar geometry.

the theoretical cases required for evaluation of the plume visibility model. For the planar geometry illustrated in Fig. 4, the latex suspension was contained in a rectangular Pyrex[®] cell 8.3 by 10.2 cm with a path length of 0.089 cm. Thus, for this scatterer geometry, the ratio of source beam diameter, d , to the thickness of the scattering medium, t , was 28.5. In the case of the cylindrical geometry illustrated in Fig. 5, the suspension was confined in a section of Pyrex tubing with an inner diameter of 1.1 mm. For this geometric configuration, therefore, the scattering path length, t , was 1.1 mm, and the resulting ratio, d/t , was 23.1. Optical depths are discussed in a later section.

For a chamber of this type, the experimental scattering angle, θ_E (shown in the scattering plane of Fig. 4, for example), at which the detector is placed, differs from the

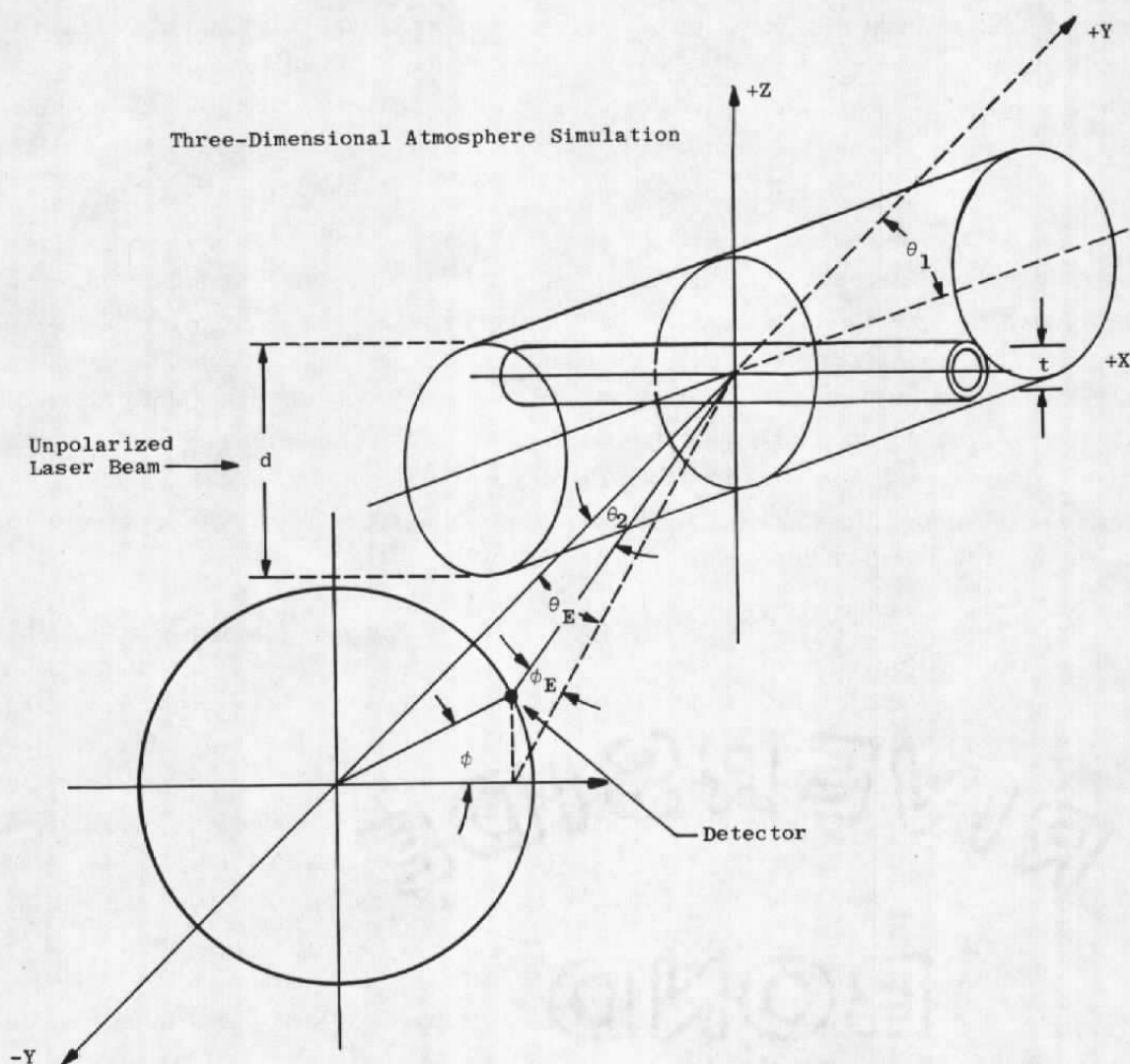


Figure 5. Light-scattering apparatus—cylindrical geometry.

actual scattering angle, θ , since refraction effects occur at the cell wall, so that

$$\sin \theta = \sin \theta_E / \eta_{H_2O} \quad (1)$$

where η_{H_2O} is the refractive index of the water. As a result, such a cell suffers a severe restriction on accessible scattering angle, θ , and is limited approximately to the 0- to 48-deg range. This limitation was removed by the surrounding of the light-scattering cell with a cylindrical outer jacket into which an index matching fluid (glycerine) was introduced. This fluid was selected because it has the same index of refraction as the inner cell walls and the cylindrical outer jacket have. The glycerine thus serves two

purposes: It eliminates most of the reflections that occur at the cell interfaces, and it results in the containment of all actual scattering angles, θ , in this plane between 0 and 90 deg within the experimental angles 0 to 65 deg. The above relation now becomes

$$\sin \theta = \left(\eta_G / \eta_{H_2O} \right) \sin \theta_E \quad (2)$$

where η_G is the refractive index of the glycerine. However, the refractive index gain in angle is not nearly as advantageous for angles perpendicular to this scattering plane. It is easily seen that for the ideal experimental case mentioned above (e.g., in which $\phi_E = 0$ deg) the scattered ray within an index matching fluid always emerges normal to the outer chamber interface so that no further refractive change must be taken into account. However, for cases in which ϕ_E is not to be confined to 0 deg, the situation becomes more complex, and care must be taken to ensure that the effects of the boundaries of the index matching fluid and outer-cell, and that of the outer-cell and air be taken into account in the determination of actual scattering angle.

The cylindrical outer chamber was constructed from a length of Pyrex tubing 12.7 cm in diameter. A section of the curved surface was removed and replaced with a plain piece of optical quality glass secured by an epoxy resin adhesive. This glass plate provided a normal surface for the injection laser source beam. Throughout this series of measurements this geometrical relation between the outer-cell injection plate and the incident beam was maintained. Variation in injection beam angle was accomplished through the rotation of the inner cell about the common axis of the inner and outer cells. A Plexiglas® plate with alignment markings was attached to the bottom of the tube which allowed alignment of the θ_E axis of rotation of the detector unit along the axis of the cylindrical tube and placement of the plane entrance window normal to the source path radiation. The center of the inner rectangular/cylindrical cell was then located on both the θ_E axis and the ϕ_E (where $\theta_E = 0$ deg) axis of the receiver unit as indicated by the origin of the coordinate system in Figs. 4 and 5, respectively. For the case of the planar geometry, the rectangular inner cell was centered along the Z axis in the X-Z plane. In the case of the cylindrical geometry, the Pyrex tube was centered on the X axis, again in the X-Z plane.

The comparison of the constructed experimental systems with the experimental configurations required for model evaluation (shown in Figs. 4 and 5) demonstrates a difference only in the definition of the experimentally measured angles (with those required by theory). Both sets of angles—the desired angles (θ_2 , ϕ) and those experimentally measured (θ_E , ϕ_E) which are measured with an uncertainty of ± 0.5 deg—are shown in both of the figures. The conversions between the sets are listed in Fig. 6. The inner chambers were secured by a separate mounting assembly providing independent alignment of this cell with respect to the incident laser beam.

CONVERSIONS:

EXPERIMENTAL ANGLES θ_E AND ϕ_E to θ_2 and ϕ

$$\theta_2 = \tan^{-1} \tan^2 \theta_E + \frac{\tan^2 \phi_E}{\cos^2 \theta_E}^{1/2}$$

$$\phi = \tan^{-1} \frac{\tan \phi_E}{\sin \theta_E}$$

or

$$\theta_E = \tan^{-1} (\cos \phi \tan \theta_2)$$

$$\phi_E = \sin^{-1} (\sin \phi \sin \theta_2)$$

Figure 6. Experimental/actual scattering—angle conversion.

2.3 SCATTERING DETECTOR SYSTEM

The scattered-light detection system is shown schematically in Fig. 7. For the experimental configuration to simulate most closely the desired physical conditions, it was necessary to ensure that the scattered radiation received by the photomultiplier detector originate entirely from within the illuminated volume; i.e., it was necessary that the detector be focused on the center of the scattering volume and have a field-of-view much narrower than the width of the incident beam. These requirements were met by using a very wide incident beam of parallel radiation, very small apertures in the receiver path to define a narrow cone of scattered light, and a short path length of the scattering medium. The receiver system utilized in these measurements consisted of two defining apertures, a focusing lens with a focal length of 20.3 mm, and an EMI 9502B photomultiplier tube with an S-11 spectral response and a 10-mm-diam photocathode surface. The tube was contained in a light-tight housing especially constructed to support the receiver optical system as well as the phototube assembly. The two apertures, both 1 mm in diameter, were separated by 30.2 cm; the first aperture was mounted 15.1 cm from the center of the scattering volume. As a result, the subtended field-of-view at the center of the scattering volume was approximately 2.0 mm in diameter. The scattered radiation collected through the defining apertures was then focused through the use of the lens onto the active surface area of the photomultiplier. Power for the photomultiplier was supplied by a well-regulated, highly stable Fluke 405B power supply.

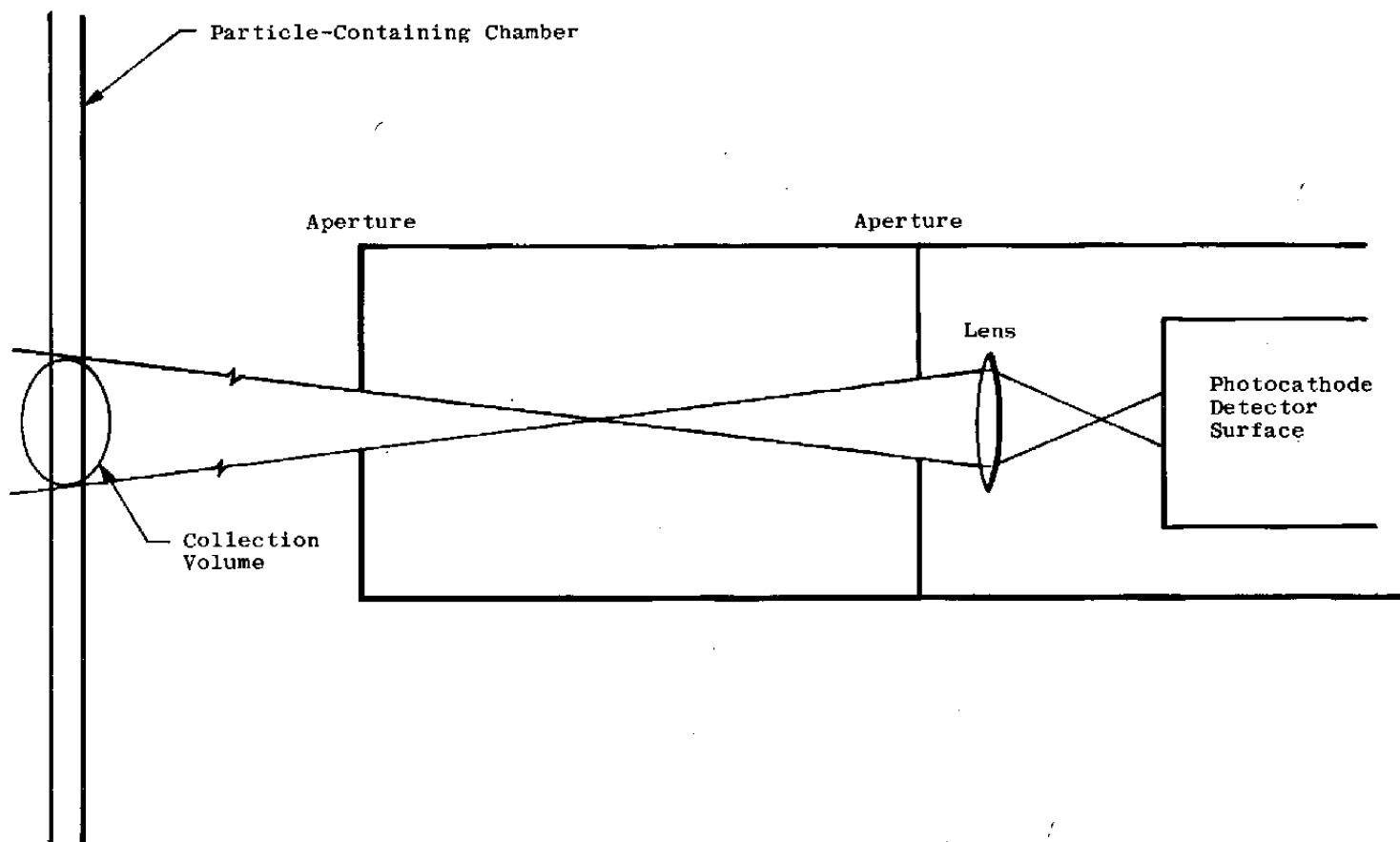


Figure 7. Receiver optical system.

The output of the photomultiplier was processed by a photon-counting system that included an amplifier, discriminator, dual counter-timer, and a rate meter. The rate meter output was displayed and recorded with both a strip-chart recorder and a multichannel analyzer that was operated in the multichannel scaling mode. Subsequent data processing was performed using an IBM® 370/165 computer.

2.4 SAMPLE PREPARATION

The light-scattering measurements were performed on aqueous suspensions of polystyrene latex spheres. The average diameters of the spheres in the monodispersions and polydispersions utilized throughout the course of the study were in the 0.1- to 1.0 μ m range. However, the illustrations in this report are limited to those particles with an average diameter determined by electron microscopy to be 0.220 μ m and with a standard deviation of 0.0065 μ m. The density of the latex spheres was 1.05 gm/ml. The refractive index determined by the Cauchy dispersion relation (Ref. 1) was

$$\eta = A + B/\lambda^2 + C/\lambda^4 \quad (3)$$

where λ is the wavelength of the incident radiation in the scattering medium in μ m and the Cauchy relation constants are

$$A = 1.5663, B = 7.85 \times 10^{-3} (\mu\text{m}^2), \text{ and } C = 3.34 \times 10^{-4} (\mu\text{m}^4) \quad (4)$$

Thus, for a series of measurements made with an Ar⁺ laser operating at 514.5 nm in air (0.3853 μ m in the suspension),

$$\eta_{\text{latex}} = 1.634$$

and

$$\eta_{\text{eff}} = \eta_{\text{latex}} / \eta_{\text{H}_2\text{O}} = 1.224 \quad (5)$$

The size parameter, α , is given by

$$\alpha = \pi D / \lambda \quad (6)$$

where D is the particle diameter and $\alpha = 1.7938$. The extinction coefficient, Q_{ext} , was then found to be 0.2300. The value of the scattering cross section, σ_{scat} , was then determined from

$$\sigma_{\text{scat}} = (D/2)^2 Q_{\text{ext}} = 8.741 \times 10^{-11} \text{ cm}^2 \quad (7)$$

For each experimental series corresponding to a desired optical depth, the suspension was prepared by using the stock solution of Dow Chemical and diluting its

known concentration, n_p , to the desired particle concentration, n_{ps} . The n_{ps} concentration (particles/cc), after s dilutions of the stock solution of concentration n_p is given by

$$n_{ps} = n_p \left(V_{T_0} / V_{T_s} \right) \prod_{i=1}^s \chi_i \quad (8)$$

where V_{T_0} is the original stock volume of density n_p , V_{T_s} is the volume of the s th dilution, and $V_{T_s} = \chi V_{T_{s-1}} + V_{H_2O}$ (added on s dilutions); χ_i is the fraction of volume taken from the $(i-1)$ th dilution.

The volumetric dilutions were made through the addition of filtered, doubly distilled, de-ionized water, and the concentration was adjusted to any desired value by the addition of such purified water.

The diluted sample was transferred by pipette to a clean light-scattering cell. With the cell and pipette in contact near the cell's edge, the cell was filled. Filling continued slowly, to prevent foaming, until the suspension was within approximately 5 mm of the cell top. When full, the cell was fitted with a glass cover so that there was no cell-cover interaction near the suspension. No evaporation or capillarity losses were observed during the course of a typical series of experiments. To investigate potential settling problems, a diffusion/sedimentation order-of-magnitude computation was performed to investigate the potential of particulate sedimentation which would place constraints on the data acquisition time available before stratification. These calculated results and the excellent reproducibility of results over long experimental data acquisition periods indicated no significant particle sedimentation effects.

All glassware was thoroughly cleaned, initially with fresh potassium dichromatic sulfuric acid cleaning solution and then rinsed with large quantities of distilled, de-ionized, particulate-free water. No tap water was allowed to come in contact with the glassware at any time after initial cleaning. All containers and instruments were repeatedly cleaned with the cleaning solution, steam rinsed, and finally rinsed with the particulate-free water to ensure good results. The light-scattering cell was cleaned in like manner, and all glassware was dried under an oil-free gaseous helium purge filtered to 0.47 μ m. Cell and glassware sanitation could be monitored easily through examination under input beam illumination.

The particulate-free water was produced by successive vacuum filtration and by boiling, using 25 Å Millipore® filters. Washing of glassware, using progressively more particulate-free stock water in each step, provided excellent water quality throughout the period of sample preparations. At least five successive 25 Å Millipore filtrations were performed before a water sample was declared particulate free.

2.5 TRANSMISSION MEASUREMENTS

Another experimental technique, based on transmission measurements, was used during this experimental program. In this case the intensity of the beam of light passing through the suspension of spherical scatterers is attenuated as a result of the incident electromagnetic radiation scattering. The fractional decrease in the intensity of the incident radiation as it traversed a single-scattering region is given by the relation (Beer's Law) (Ref. 2)

$$\frac{-dI}{I} = \sigma_{\text{scat}} N dx \quad (9)$$

where, again, σ_{scat} is the scattering cross section per particle, N is the number of scatterers per unit volume (cm^3), and x is the path length through the scatterers. Integration of Eq. (9) yields

$$I/I_o = \exp(-\sigma_{\text{scat}} Nx) \quad (10)$$

where I_o is the incident intensity.

From Eq. (10) the optical depth is defined by

$$\tau = N x \sigma_{\text{scat}} = \ln(I_o/I) \quad (11)$$

Further, for a spatially isotropic, monodisperse or polydisperse particle sample of known distribution function, index of refraction, and fixed path length, x , the measurement of the intensity ratio, I/I_o , yields a measurement of the number density of the scatterers according to the relation

$$N \text{ cc}^{-1} = \ln(I_o/I) / x \sigma_{\text{scat}} \quad (12)$$

With the maintenance of a fixed path length, x , the concentration of a monodisperse distribution of spherical latex particles was varied to cover the optical depth range from 0.073 to 2.0. Figure 8 shows the variation of the transmission ratio, I/I_o , with concentration and optical depth for a $\sim 220\text{-}\mu\text{m}$ particle diameter. Figure 8 shows that deviation of the transmission ratio from the Beer's Law dependence occurs for $\tau \gtrsim 0.12$. Consequently the $\tau \lesssim 0.12$ concentrations represent single-scattering configurations, whereas multiple scattering is significant for the $\tau \gtrsim 0.12$ concentrations.

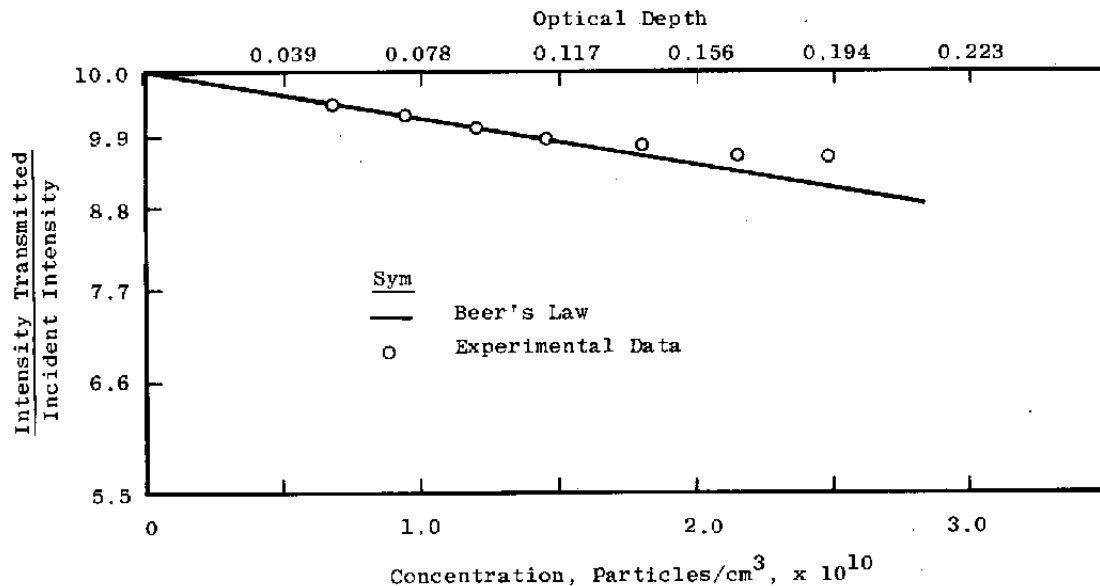


Figure 8. Transmission results for 0.220- μ m-diam particles.

2.6 DATA ACQUISITION PROCEDURE

Once the light-scattering cell was cleaned and filled with an appropriate suspension, experimental runs were made using a procedure developed during a series of Mie-scattering code verification experiments performed at AEDC. The incident beam intensity was measured using the Coherent Radiation power meter, which was mounted in a standard (or reference) position. Cell transmission was measured; then the inner cell was placed in its mount and adjusted for proper tilt angle. (Note that a range of incident laser angles was used throughout the experimental series). Data runs were then made by varying the detector's scattering angle and recording the detected scattering intensity as a function of incident laser polarization, power, and detector polarization. A constant monitoring of incident laser power was performed to ensure that corrections for incident power fluctuations could be made, if required; repeated scans of known cases were made to verify temporal invariance of the integrity of the sample.

3.0 RESULTS AND DISCUSSION

Reduction of the experimentally acquired data was performed with an IBM 370/165 computer routine that included corrections for all experimental factors that could affect system calibrations. Specifically, (1) variations in the sample scattering volume with detector scattering angle, (2) reflection losses at all boundaries within the experimental apparatus, (3) the effects of photomultiplier pulse buildup (dead time), (4) stray light contributions, and (5) background scattering effects had to be carefully accounted for in order to produce accurate results. These correction terms will be discussed individually, and both experimental multiple- and single-scattering data examples will be presented.

3.1 CORRECTIONS TO DATA

For the experimental arrangement utilized in this study, the effective volume, $V(\theta, \phi)$, from which the Mie/multiple-scattered radiation enters the detector apertures, is a function of the scattering angle. Since it was desired that the experimental data be free of scattering volume effects, an accurate determination of this variation in source volume with scattering angle was necessary so that its effect could be included in the data reduction procedure. Therefore, a geometric ray-tracing analysis was performed for the collection optics/chamber system, and the resulting angular variation of the effective scattering volume was included in the computer data reduction routine.

To illustrate the effect of this variation of the effective volume, consider the experimental geometry shown in Fig. 4 for the case in which $\phi = 0$ deg. Since the radiation detected by the photomultiplier originates entirely within the illuminated volume of the scattering solution, the effective volume changes with scattering angle, θ_2 , as

$$V(\theta_2, 0) \cos \theta_2 = \text{Constant} \quad (13)$$

The effect of reflection losses at each air-Pyrex, Pyrex-glycerine, and Pyrex-suspension boundary was calculated using the Fresnel relations (Ref. 3) for a dielectric interface. These reflection-loss factors were determined for both incident laser and scattered ray paths and were included in the data reduction computer routines; however, the factors were significant only at large scattering angles.

In all measurements made in this study, contributions to the angular scattering intensities from the solvent and glycerine were negligible. Stray light contributions caused by direct scattering from the walls of the glass scattering chambers, however, were large enough to be considered in certain cases. To account for this background radiation, the angular scattering pattern of the chamber system with the sample cell filled with particulate-free water was recorded; this is shown in Fig. 9 along with a low particulate concentration, experimental scan for comparison. For the directly scattered radiation, this background could be subtracted from the scattering intensities. However, this correction is important only for very low suspension concentrations since the stray light is rapidly attenuated as the suspension concentration increases.

The contribution of wall-scattered radiation to the total scattering signal was found to be negligible for both the single- and multiple-scattering cases. That this is the case can be seen by considering the background radiation intersecting the particulate sample. The radiation scattered by the individual particles is projected into 2π steradians, whereas the detector's collection solid angle is only 3.44×10^{-5} steradians. The contribution to the scattering signal is, thus, orders of magnitude lower than the actual scattering signal.

Mie Scattering Data - Single Scattering

 $d = 1.091 \mu$ Monodispersion (Dow latex)

 $n_p = 1.4074 \times 10^6 \text{ cc}^{-1}$
Sym

- Experimental Data (No Background Correction), Vertical Polarization
- △ Experimental Data (Background), Vertical Polarization
- Theory, Vertical Polarization

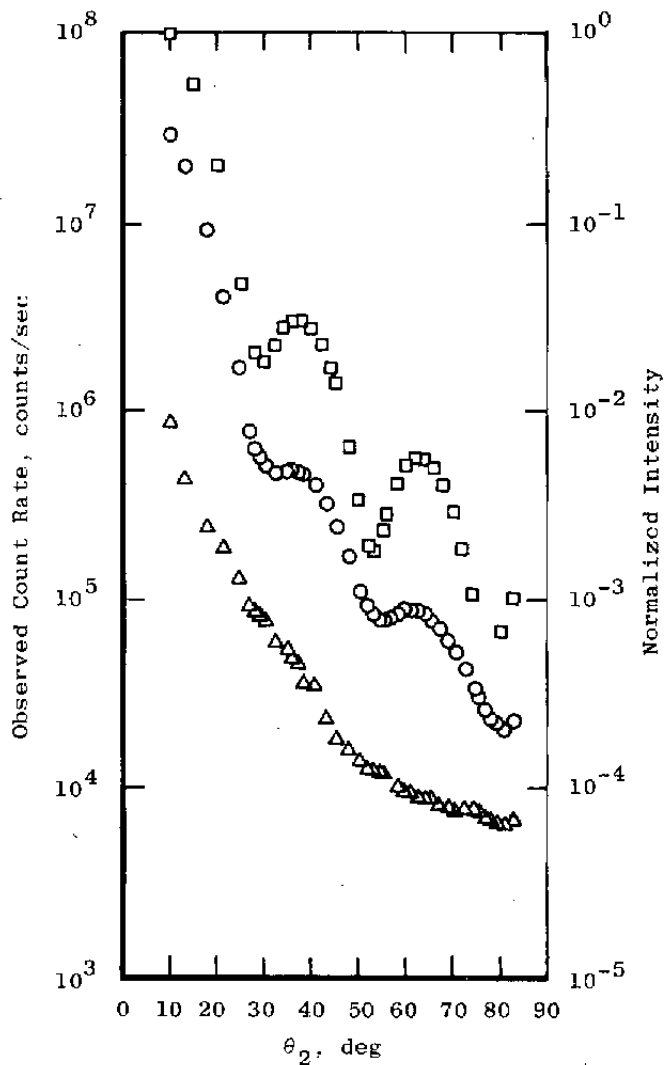


Figure 9. Single-scattering data comparison with stray light background.

Finally, the effects of nonlinear photomultiplier response with scattering intensity were accounted for through standard photon-counting dead-time connections.

3.2 SAMPLE DATA

To verify the operation of the system and the accuracy of the data acquisition and correction procedures, single-scattering data were acquired for monodisperse distributions of spherical particles of 0.220- and 1.091- μm diameters. Shown in Fig. 9 is the angular variation of the scattered intensity (vertical polarization) for the sample containing 1.091- μm -diam particles. The particle number density for this sample was $1.407 \times 10^6 \text{ cc}^{-1}$. Also included in this figure are the angular scattering pattern from a background sample of particulate-free water and the Mie scattering predictions for the 1.091- μm -diam particles. By subtracting the background signal from the experimental data of Fig. 9, the Mie scattering results shown in Fig. were obtained.

Many data for a wide variety of conditions were accumulated throughout this study. Incident laser wavelengths were ranged from 514.5 to 610.3 nm; incident laser injection angles were varied from 0 to 45 deg; both detector scattering angles θ_2 and ϕ were varied; and several optical depths (0.073, 0.5, and 1.0) were utilized for both monodisperse and polydisperse particle suspensions. Figures 11, 12, and 13 present additional data for the $D = 0.220\text{-}\mu\text{m}$ particles at three optical depths for the geometry of Fig. 4 ($\phi = 0$). Figures 14, 15, and 16 present similar cases for the 0.220- μm particles for the geometry of Fig. 5.

4.0 CONCLUSIONS

To provide experimental verification of multiple-scattering Mie theoretical prediction, measurements were made of the scattering of laser radiation by spherical particles of known index of refraction and monodisperse size distribution function. The particle diameter range studied was 0.220 to 1.001 μm , and the monochromatic, laser source wavelength range used was 514.5 to 610.3 nm. The particle concentration was varied over a range sufficiently broad to enable variation of the optical depth, τ , over the range of 0.073 to 2.0. This range of particle concentration included both the single- and multiple-scattering regions. Comparison of the experimental single-scattering results with the Mie-scattering, theoretical predictions showed agreement well within experimental error. Finally, the angular variation of multiple-scattered radiation was obtained for experimental configurations that simulated solar scattering by planar and cylindrical gas/particle samples.

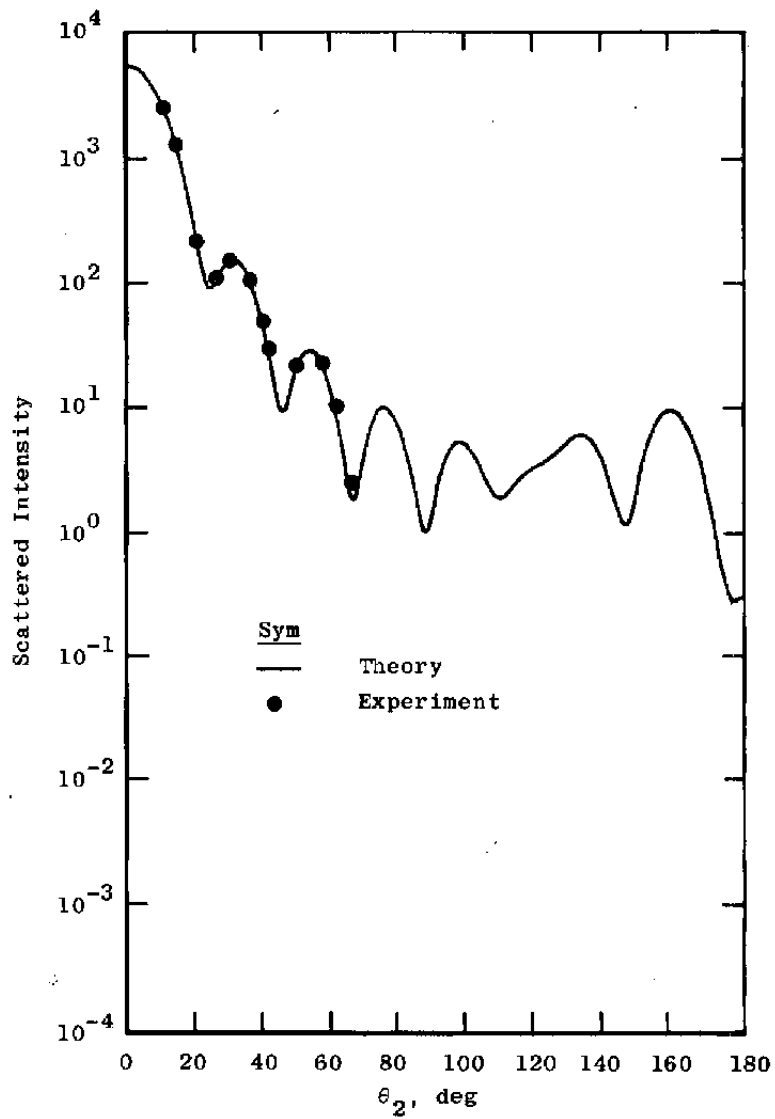


Figure 10. Single-scattering alignment comparison.

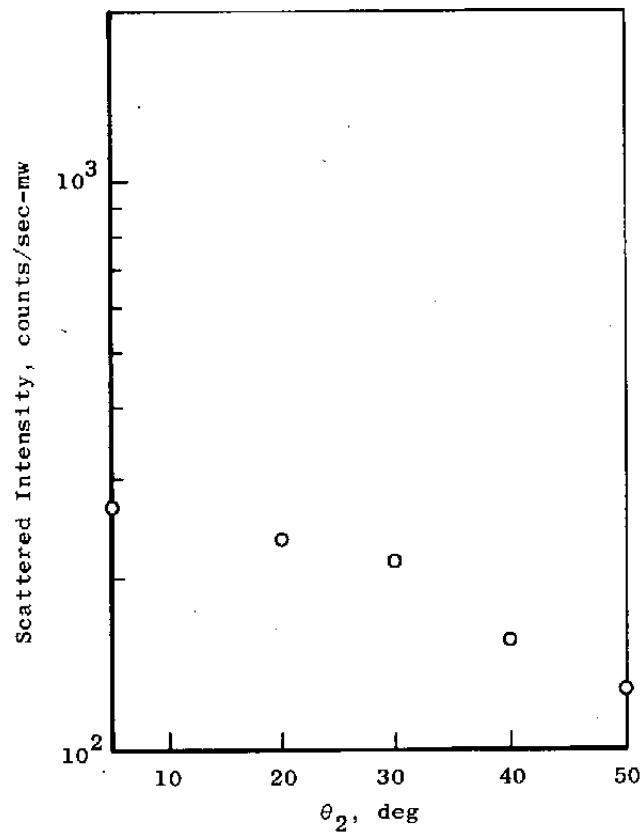


Figure 11. Experimental data, planar geometry,
 $\tau = 0.073$.

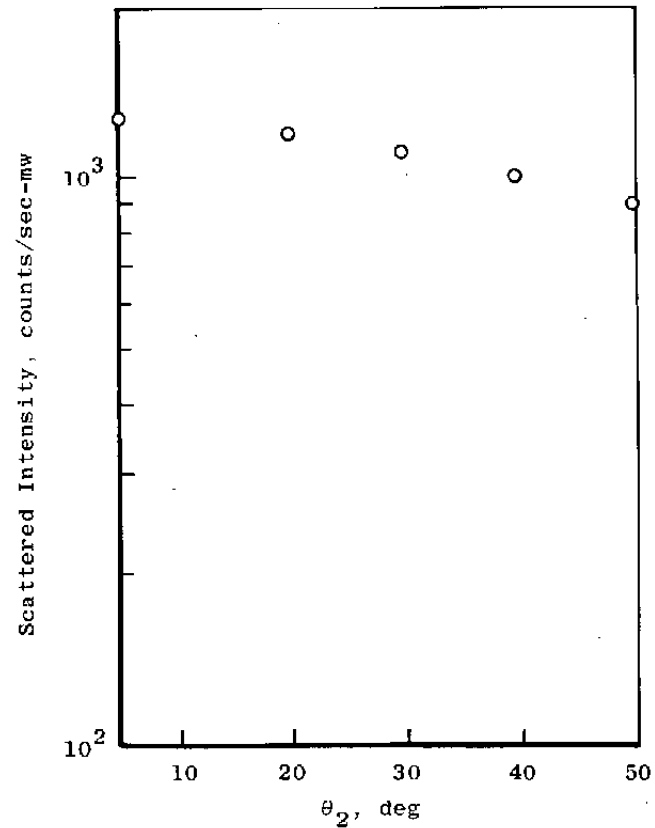


Figure 12. Experimental data, planar geometry,
 $\tau = 0.50$.

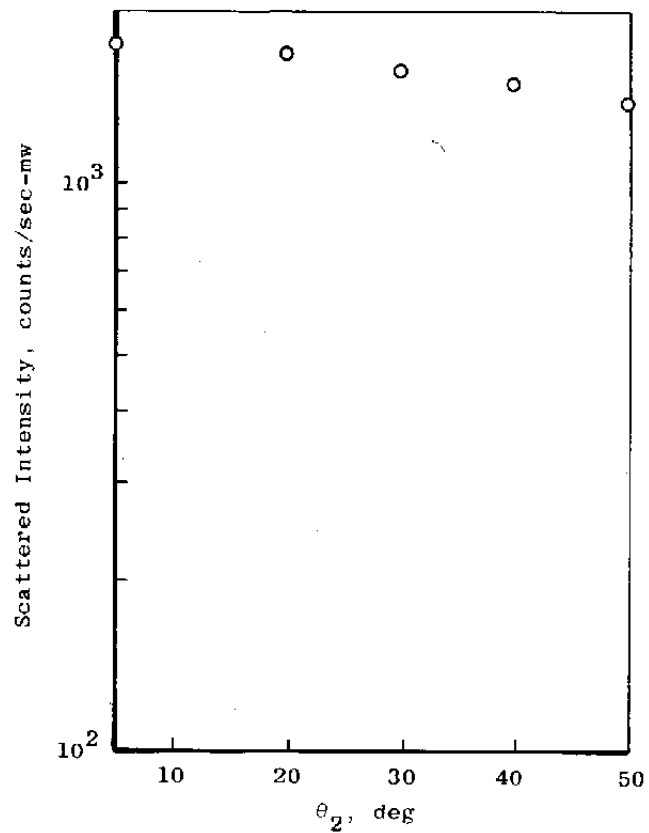


Figure 13. Experimental data, planar geometry,
 $\tau = 1.00$.

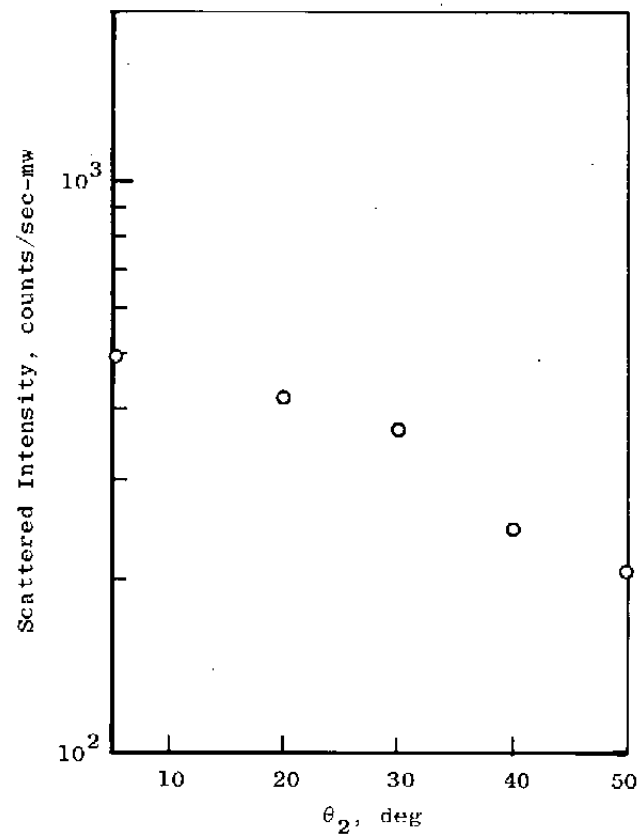


Figure 14. Experimental data, cylindrical geometry,
 $\tau = 0.073$.

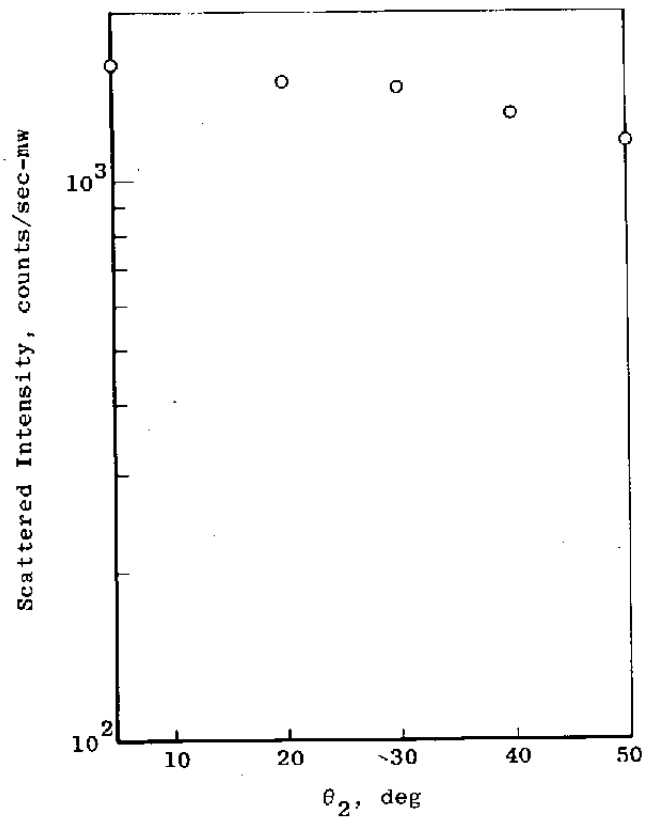


Figure 15. Experimental data, cylindrical geometry, $\tau = 0.50$.

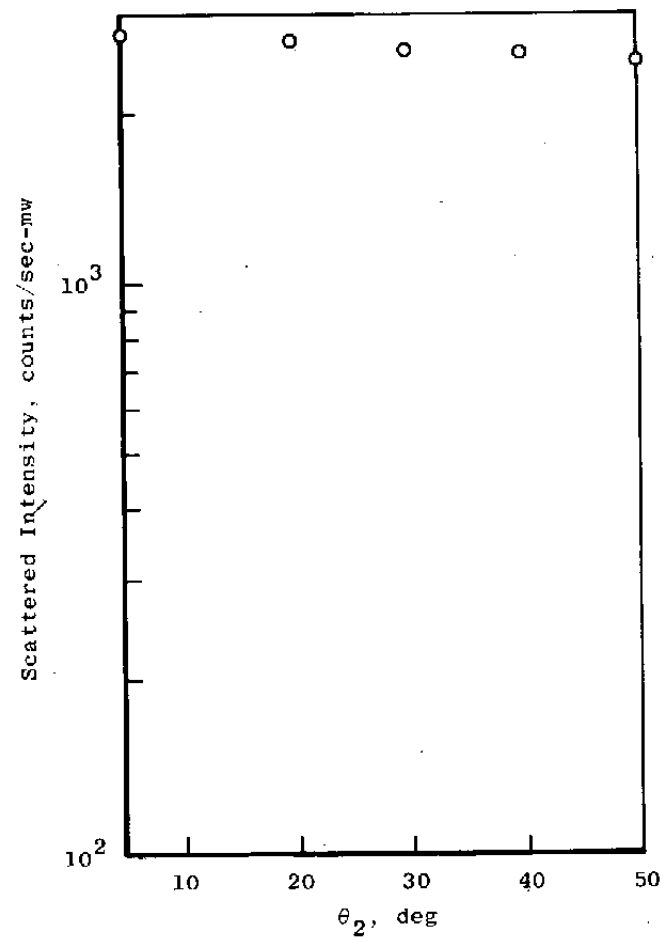


Figure 16. Experimental data, cylindrical geometry, $\tau = 1.00$.

REFERENCES

1. Jenkins, F. A. and White, H. E. Fundamentals of Optics. Third Edition. McGraw-Hill, New York, 1957.
2. Wood, R. W. Physical Optics. Third Revised Edition. Dover Publications, Inc., New York, 1967.
3. Born, M. and Wolf, E. Principles of Optics. Fourth Edition. Pergamon Press, Oxford, New York, 1970.
4. Lewis, J. W. L., Curry, B. P., and Weaver, D. P. "Determination of the Size Distribution Function for Particles in a Hypersonic Flow Field." AEDC-TR-77-101 (AD-A056923), July 1978.

NOMENCLATURE

A, B, C	Cauchy relation constants
D	Particle diameter, μm
d	Source beam diameter, mm
I	Incident laser power, watts
I_0	Incident intensity
N_n	Particle number per unit volume ($1/\text{cm}^3$)
n_p	Known concentration of stock solution (Dow Chemical)
n_{LPS}	Desired particle concentration of stock solution
Q_{ext}	Extinction efficiency ratio
t	Thickness of particle cells, mm
V_T	Total volume, mm
V_{T0}	Original stock volume of density n_p
V_{Ts}	Volume of the sth dilution
$V(\theta, \phi)$	Effective scattering volume
x	Laser path length through scatterers
θ	Accessible scattering angle, deg
θ_E	Experimentally measured polar scattering angle, deg
θ_1	Incident laser angle, deg
θ_2	Polar scattering angle, deg
α	Particle size parameter, dimensionless
η	Index of refraction
λ	Wavelength of incident radiation in scattering medium, μm

σ_{scat}	Scattering cross section
τ	Optical depth
ϕ	Azimuthal scattering angle, deg
ϕ_E	Experimentally measured azimuthal scattering angle, deg
χ_i	Fraction of volume taken from the (i-1)th dilution

SUBSCRIPTS

G	Glycerine
O	Stock solution value
P	Particles
eff	Effective value
H ₂ O	Water
latex	Latex spheres
s	sth dilution of total volume [Eq. (8)]